Preferential Control of Forward Reaction Kinetics in Hydrogels Crosslinked with Reversible Conjugate Additions

Thomas M. FitzSimons,[1] Felicia Oentoro,[1] Tej V. Shanbhag,[1] Eric V. Anslyn,[2] Adrianne M. Rosales[1*]

[1] McKetta Department of Chemical Engineering, University of Texas at Austin, Austin, TX, USA

[2] Department of Chemistry, University of Texas at Austin, Austin, TX, USA

For Table of Contents use only:

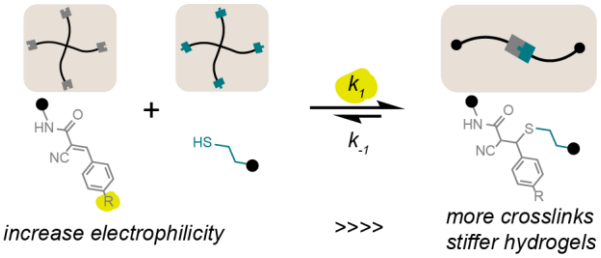

Abstract

Molecular substitutions were used to demonstrate preferential control over the kinetic rate constants in a poly(ethylene glycol)-based hydrogel with two different reversible thia-conjugate addition reactions. A strong electron withdrawing nitrile group on the conjugate acceptor showed a 20-fold increase in the forward rate constant over a neutral withdrawing group, while the reverse rate constant only increased 6-fold. Rheometry experiments demonstrated that the hydrogel plateau modulus was primarily dictated by reaction equilibrium, while the stress relaxation characteristics of the hydrogel were dominated by the reverse rate constant. Furthermore, the dynamic crosslinking allowed the hydrogel to rapidly and spontaneously self-heal. These results indicate that decoupling the kinetic rate constants of bond exchange allow systematic control over dynamic covalent hydrogel bulk properties, such as their adaptability, stress relaxation ability, and self-healing properties.

Introduction

Hydrogels crosslinked with dynamic bonds have shown promising properties for applications such as tissue engineering, drug delivery, and 3-D printing.[1–7] In particular, dynamic bonds confer adaptability to the network, enabling rearrangement on the molecular scale that is dependent on bond lifetime and reaction kinetics.[8,9] This rearrangement can be translated to several useful bulk properties, such as the ability to relax an applied stress or re-form crosslinks across an induced network defect.[10–14] Furthermore, dissociation of dynamic crosslinks may lead to shear-thinning behavior and enhanced injectability.[15–17] For these reasons, engineering bulk hydrogel properties via molecular-level control of dynamic crosslink reactivity has been the subject of intense recent interest.

Dynamic crosslinking chemistries span both non-covalent and covalent bonds. Non-covalent interactions include metal coordination,[18,19] physical entanglement,[20] hydrogen bonds,[21–24] and guest-host complexes.[25] Guest-host complexes in particular have shown a wide range of binding affinities (K_{eq} ~ 10^2-10^{12} M^{-1})[26] and tunable kinetic parameters for binding that directly translate into a breadth of time-dependent hydrogel mechanics.[27] Dynamic covalent crosslinking, on the other hand, includes a smaller set of explored reactions with slower kinetics,[28] although these are still of intense interest for their robust mechanical properties in polymer networks.[29–32] Despite this recent interest, studies relating systematic variation of bond exchange kinetics to hydrogel properties are limited.

Some dynamic covalent chemistries have been extensively investigated as hydrogel linkages, including hydrazone[8,31,33,34] and boronic ester[4,11,35,36] groups, and emerging reports suggest that control over reaction kinetics can have dramatic and tunable effects on the resulting hydrogel properties.[37,38] For instance, in the case of reversible hydrazone crosslinking, a change from an aliphatic aldehyde to a benzaldehyde can significantly slow the forward and reverse rate constants of exchange by two orders of magnitude, leading to slower stress relaxation in hydrogels.[33] In another hydrazone crosslinking example, bond exchange kinetics were

temporarily accelerated with the use of a benzimidazole-based catalyst, which enhanced hydrogel injectability for cell delivery applications.[39] A third example altered reaction kinetics, and therefore the equilibrium binding constant, using the *E*/*Z* isomerization of azobenzene boronic acids to reversibly control hydrogel gel-sol transitions.[40] These reports demonstrate the impact of reversible covalent crosslink kinetics on bulk hydrogel properties, and further motivate the preferential control of the forward and reverse rate constants to tailor specific mechanical behavior.

To expand the types of reversible covalent hydrogel linkages, especially with a focus on tunable kinetic parameters, we have explored Michael addition as a dynamic crosslink chemistry. Michael addition has long been used for efficiently crosslinking hydrogels.[41–44] This reaction consists of a nucleophilic addition to an α,β-unsaturated carbonyl, typically with a thiol for the former, and an acrylate, norbornene, or maleimide for the latter. In the case of these nucleophilic acceptor molecules, the reaction is irreversible, thereby creating a static hydrogel with purely elastic material properties. Recent research has demonstrated, however, that an electron withdrawing group at the α site of the unsaturated carbonyl switches this normally irreversible reaction into a reversible one.[45,46] Subsequent to conjugate addition, deprotonation of the α-carbon, which can be facilitated by the substituent groups on the α carbon, allows the reaction to reverse. This releases a free thiol and recreates the α,β-unsaturated carbonyl by an $E1_{CB}$ mechanism. A

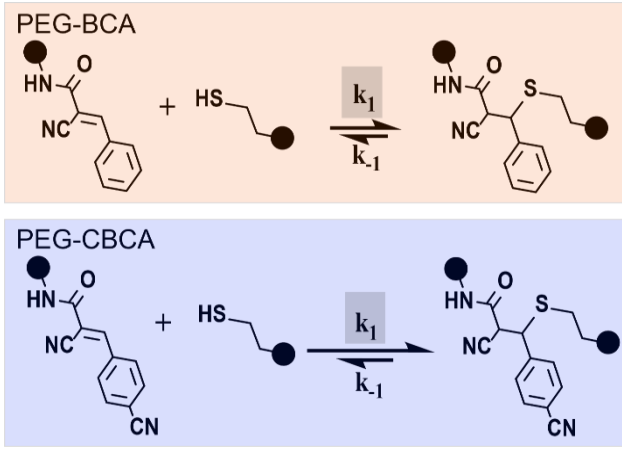

Figure 1. Reaction of an unmodified conjugate acceptor (**PEG-BCA**, in orange) and a para-nitrile modified acceptor (**PEG-CBCA**, in blue) with a thiol. Black circles represent either poly(ethylene-glycol) backbone polymers in case of hydrogel formation, or a hydroxyl group in the case of the thiol during UV/VIS spectroscopy. Because of the electron withdrawing strength of the nitrile group, k_1 increases significantly more than k_{-1}. This leads to a shift in equilibrium towards more product formation in the case of **PEG-CBCA**.

small molecule study investigating this reversible reaction revealed that electron withdrawing substitutions to an aromatic ring at the β-position could significantly increase the equilibrium constant for the reaction, presumably due to the larger k_1 resulting from enhanced electrophilicity of the reaction site.[47] In this report, we leverage the tunability of the reversible Michael addition kinetics to selectively control hydrogel mechanics.

Toward this goal, we functionalized a multi-arm poly(ethylene-glycol) (PEG) polymer with two distinct conjugate acceptor molecules (Figure 1) and performed kinetic measurements using UV/VIS spectroscopy with a small molecule thiol to prevent gelation. We demonstrate preferential control over the forward reaction rate kinetics using aromatic substituent group variants, thereby increasing the equilibrium constant while leaving the rate of dissociation relatively unchanged. We then mixed these functionalized PEG macromers with multi-arm thiol-functionalized PEG macromers, which spontaneously gelled in pH 7.4 buffer solution. Because the rate constants dominate different bulk properties, our results show that control of crosslinking kinetics is important for tuning hydrogel plateau modulus independent of stress relaxation. Furthermore, the fast exchange of the reversible Michael addition crosslinks leads to rapid self-healing behavior, which suggests utility for many hydrogel applications.

Experimental Section

Materials. All materials were used as purchased unless otherwise specified. Purchased from Sigma Aldrich: propargyl amine, anhydrous ethanol, peptide synthesis grade dimethyl formamide (DMF), phosphate buffered saline, and dimethyl sulfoxide-d_6, deuterium oxide, deuterated chloroform, copper sulfate, sodium ascorbate, and *β*-mercaptoethanol. Purchased from JenKem USA: 4-arm 20k molecular weight PEG-Azide, 4-arm 10k molecular weight PEG-Thiol. Purchased from Fisher Scientific: methyl cyanoacetate, and diethyl ether.

Synthesis of propargyl cyanoacetamide (Scheme 1). Propargyl cyanoacetamide was synthesized by adding propargyl amine (5.81 mL, 0.0908 moles, 1.0 equiv) and methyl

cyanoacetate (8.01 mL, 0.0908 moles, 1.0 equiv) to an oven dried round-bottom flask. The reaction proceeded upon stirring for 24 hours at room temperature. The product precipitated out and was washed with 200 mL of ice-cold diethyl ether under vacuum filtration. The product was a light yellow solid, yield=84%. ^{1}H NMR ($CDCl_3$, 400 MHz): δ=6.28 (s, 1H), δ=4.1 (dd, 2H), δ=3.4 (s, 2H), δ=2.29 (t, 1H). HRMS (CI) $[M+H]^+$ Calculated for C6H7N2O: 123.06. Found: 123.0558.

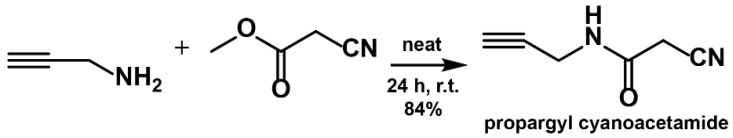

Scheme 1. Synthetic route for propargyl cyanoacetamide.

Synthesis of PEG-cyanoacetamide (PEG-CA, Scheme 2). PEG-CA was synthesized via copper-catalyzed click chemistry by adding 4 arm, 20 kDa molecular weight PEG-Azide (1 gram, 0.05 mmol) and propargyl cyanoacetamide (29.3 mg, 0.24 mmol, 4.8 equiv) to a round bottom flask. This flask was purged with argon for 5 minutes. Copper (II) sulfate (6.4 mg, 0.04 mmol, 0.8 equiv) and sodium ascorbate (15.8 mg, 0.08 mmol, 1.6 equiv) were added to a separate vial which was also purged with argon. Ultra-filtered water (8 mL) and peptide synthesis grade DMF (8 mL) were added via syringe to the vial containing copper sulphate and sodium ascorbate. The vial was sonicated to dissolve the solids. This vial was cannulated to the flask containing the PEG and propargyl cyanoacetamide. The mixture was allowed to react for 3 days under constant flow of argon. After three days, the contents were precipitated into ice-cold diethyl ether (2 vials with 30 mL ether each). The reaction mixture phase separated into a PEG-containing aqueous layer and an organic layer. The organic layer was discarded, and the aqueous layer was moved to a dialysis bag (6-8 kDa MWCO) and dialyzed against DI water for three days, changing the water every day. After three days, the contents were lyophilized. Yield=99%, Functionalization=~90%. ^{1}H NMR (DMSO-d6, 400 MHz): δ=8.68 (t, 1H), δ=7.92 (s, 1H), δ=3.4 (s, 454H).

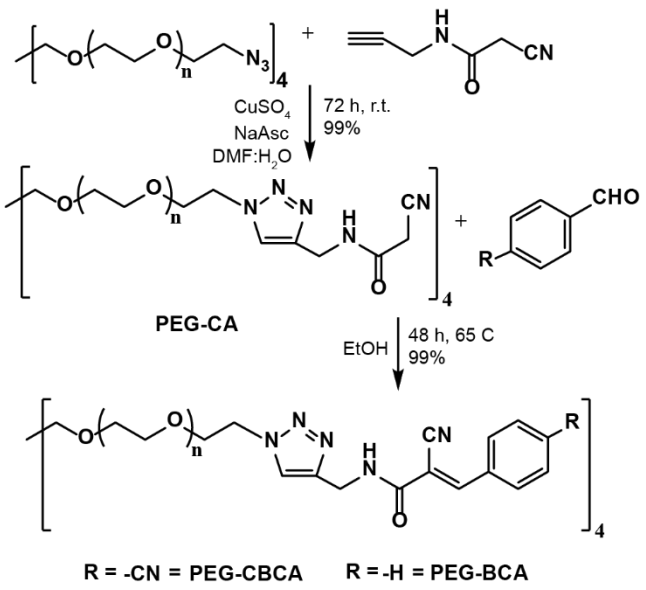

Scheme 2. Synthetic route for PEG macromers functionalized with conjugate acceptors.

Synthesis of conjugate acceptor-functionalized PEG (Scheme 2). A Knoevenagel condensation was used to attached either benzaldehyde or 4-cyanobenzaldehyde to PEG-CA to make **PEG-BCA** or **PEG-CBCA**, respectively. In either case, PEG-CA (272 mg, 0.0136 mmol) and benzaldehyde (552 uL, 5.44 mmol, 400 equiv) or 4-cyanobenzaldehyde (713 mg, 5.44 mmol, 400 equiv) were added to a round bottom flask. The flask was purged with argon. Anhydrous ethanol (5 mL) was added to the flask, which was then heated to 65 ^{o}C. The flask was purged with argon for three additional minutes. The reaction was allowed to proceed for two days. After two days, the solution was precipitated into ice-cold diethyl ether (35 mL, three times) to separate the functionalized PEG product from excess aldehyde. After each precipitation, the vial was centrifuged to recover the precipitated solid PEG product, and the supernatant was discarded. After precipitation, the solid product was dried overnight under vacuum. Yield= 99%, Functionalization=~85% for PEG-BCA and ~80% for PEG-CBCA. ^{1}H NMR (DMSO-d6, 400 MHz): **PEG-BCA**: δ=8.99 (t, 1H), δ=8.17 (s, 1H), δ=7.94 (s, 1H), δ=7.89 (dd, 2H), δ=7.51-7.56 (m, 3H), δ=3.4 (s, 454H); **PEG-CBCA**: δ=9.11 (t, 1H), δ=8.25 (s, 1H), δ=8.04 (d, 2H), δ=8.04 (d, 2H), δ=7.96 (s, 1H), δ=3.4 (s, 454H).

Rheometry. Rheometry experiments were conducted using a TA Instruments Discovery HR2 rheometer. An 8 mm flat stainless steel geometry on a stainless steel Peltier plate was used for all experiments. Hydrogels were compressed *in situ* on the rheometer to the appropriate gap

height to fill the sample space. The rapid rearrangement of the crosslinks prevented pre-straining the hydrogel. Hydrogels were surrounded with silicon oil after lowering the geometry to the experimental gap height to prevent dehydration. All experiments were done at room temperature. Frequency sweeps were performed from 0.01 to 10 rad/s at 1% strain with a 10 wt% hydrogel. Stress relaxation experiments used an initial strain of 1% with a one second rise time with a 10 wt% hydrogel. Self-healing high/low strain experiments used 500% and 0.5% strain respectively with a frequency of 10 rad/s and a 5 wt% hydrogel.

Ultraviolet/Visible (UV/VIS) Spectroscopy. UV/VIS measurements were taken on a Biotek Synergy H1 Multi-Mode Microplate Reader. All experiments were done in triplicate. The model reaction for all UV/VIS measurements was a conjugate acceptor-functionalized 4-arm 20 kDa PEG reacting with β-mercaptoethanol. The extinction coefficient for the reactant conjugate acceptor molecule was determined prior to each experiment, using the Beer-Lambert law and a known concentration and path length. The extinction coefficient for the product was determined by reacting 50 μM of the reactant conjugate acceptor with a >600 times excess of β-mercaptoethanol, which pushed the extent of reaction to 100%. The appropriate amount of excess to ensure complete conversion was determined by recording the concentration of added thiol where the absorbance at the desired wavelength ceased changing (See Supporting Information). In the case of these molecules, 150 mM thiol concentration was sufficient for complete conversion of reactant. The same calculation method as for the reactant conjugate acceptor was used to determine the extinction coefficient.

Equilibrium constants were determined by measuring the absorbance with relatively equivalent concentrations of conjugate acceptor-functionalized PEG and β-mercaptoethanol in buffer (1x PBS, pH 7.4). By using the Beer-Lambert law for a two-component system, concentrations of reactant and product were determined (see Supporting Information). These

concentrations were used to calculate the equilibrium constant for both versions of the conjugate acceptor-functionalized PEG molecule.

NMR Spectroscopy. ^{1}H NMR spectra (400 MHz) were recorded on an Agilent MR400 spectrometer.

Hydrogel Preparation. All hydrogels were formulated by mixing **PEG-BCA** or **PEG-CBCA** with a 1:1 stoichiometric amount of thiol-functionalized 4-arm 10k molecular weight PEG. The final mixture contained 10 wt% polymer with functional group concentration around ~10 mM with variations resulting from slightly different conjugate acceptor functionality. The high/low strain rheometer experiment used a 5 wt% hydrogel. Due to the rapid reaction rates, gelation occurred too rapidly for any vortexing or pipette mixing. The hydrogels were instead mixed manually post-gelation, and due to their self-healing behavior were able to rapidly reform into a continuous hydrogel for further experimentation.

Results and Discussion

Although the reversible Michael addition reaction has been extensively investigated in small molecule systems, few reports examine the utility of this reaction in polymeric networks or hydrogels.[48,49] Here, we investigate the impact of controlled rate kinetics on the rheological behavior of PEG hydrogels crosslinked with a dynamic thia-conjugate addition reaction (Figure 1).

Synthesis and Equilibrium Constant Measurements with a Small Molecule Thiol To probe the effects of aromatic substituents on the reversible thia-conjugate addition reaction kinetics, we first synthesized two distinct PEG macromers functionalized with benzalcyanoacetamide acceptors: one containing the electron withdrawing nitrile group in the para position of the aromatic (**PEG-CBCA**), and one without any aromatic substituents (**PEG-BCA**). We developed a progressive synthesis method for PEG functionalization that proceeded via two steps (Scheme 2). In the first

step, N-propargyl cyanoacetamide (Figure S1) was attached to a 4-arm PEG-azide using copper-catalyzed cycloaddition in water with functionalization of ≥90% (Figure S2). A subsequent Knoevenagel condensation with the substituted benzaldehyde completed the conjugate acceptor. Analysis by ^{1}H NMR spectroscopy indicated high functionalization of the PEG macromer in excess of 80%, as indicated by the emergence of the amine, triazole, and aromatic hydrogens (Figures S3 and S4). Furthermore, the high molecular weight of the PEG conferred water solubility to the conjugate acceptor, allowing subsequent studies to be conducted in buffered aqueous solution.

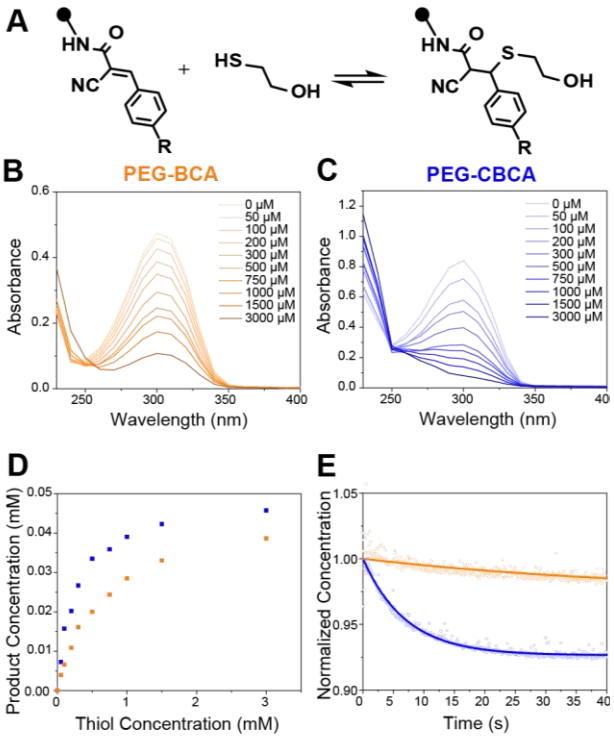

Figure 2. Equilibrium and kinetic studies for both conjugate acceptors. (A) General reaction scheme between the conjugate acceptor and β-mercaptoethanol. (B,C) Absorption spectra of **PEG-BCA** and **PEG-CBCA** with increasing concentrations of thiol. The reactant absorbs strongly at 300nm, while the product does not. (D) Product concentration as a function of thiol concentration for **PEG-BCA** (orange) and **PEG-CBCA** (blue). The maximum for both molecules is 0.05 mM. **PEG-CBCA** reaches this maximum more quickly, demonstrating that it has a larger equilibrium constant. (E) Product concentration for **PEG-BCA** (orange) and **PEG-CBCA** (blue) as a function of time. Fitting the data to a 2nd order kinetic model provides the forward and reverse rate constants.

As a first assessment of the substituent impact on covalent bond formation, we measured the equilibrium constant using a fixed concentration of conjugate acceptor (50 μM) with different amounts of a small molecule thiol, β-mercaptoethanol (Figure 2A). Both the conjugate acceptor and the product contain an absorption peak at 300 nm due to the highly conjugated π-bond system. Because the addition of the thiol breaks much of this conjugation, the absorbance at this wavelength for the product is significantly lower than for the reactant. Due to absorption being additive for multiple species, the total absorption is

the sum of the conjugate acceptor and product species. The reactant conjugate acceptor extinction coefficient is determined by measuring the 300 nm absorbance of the reactant prior to each experiment. Combining this with our experimentally determined extinction coefficients for the product (Figures S5-S8), we calculated the concentration of all species using the Beer-Lambert equation (Equation S1).

Figures 2B and 2C show absorption spectra for 50 μM of conjugate acceptors mixed with different amounts of thiol (ranging from 50-3000 μM) after 10 minutes to ensure the reaction reached equilibration. As thiol concentration increases, more reactant converts to product (Figure 2D). Dividing the concentration of products to reactants yields the equilibrium constant for both molecules, which we found to be $4.1 \times 10^3 \pm 600\ M^{-1}$ for **PEG-CBCA** and $1.2 \times 10^3 \pm 200\ M^{-1}$ for **PEG-BCA** (Table 1). A previous study that investigated this reaction with two small molecule reactants found equilibrium constants of 2700 M^{-1} for a para-nitro substituted acceptor and 390 M^{-1} for a non-substituted acceptor.[47] Their experiment involved determining reactant and product concentrations via ^{1}H-NMR spectroscopy in a pD 7.0 buffered solution of CD_3CN/D_2O (5:6). Because water is expected to solvate the thiol of β-mercaptoethanol, and there is no thiol in the product, different aqueous solvent systems would presumably affect any measured equilibrium values. Nitro groups are also more strongly electron withdrawing than a nitrile group, and our experiment held the pH constant at 7.4, which should increase kinetic rates. Given these three considerations, there is reasonable agreement between prior studies and this work.

It should also be noted that at longer time scales the acceptor hydrolyzes along the double bond at the reactive site in a reversal of the Knoevenagel condensation reaction that adds the aromatic aldehyde. The **PEG-CBCA** hydrolyzes considerably faster than **PEG-BCA** (approximately 4 times faster, Figures S9 and S10), and the addition of a thiol that can compete with this hydrolysis significantly reduces the rate of hydrolysis, by factors of 3 and 4 in the case of **PEG-CBCA** or **PEG-BCA**, respectively (Figures S11 and S12). For **PEG-CBCA** conjugated to a thiol in pH 7.4 buffer, this translates to a stability half-life of 1.9 days. Interestingly, the half-life

for conjugated **PEG-BCA** in pH 7.4 buffer was 12.7 days, a 6.6-fold difference. For this reason, we focused on bulk studies at much lower timescales to ensure our hydrogel measurements were not significantly impacted by hydrolysis.

Kinetic Studies with β-Mercaptoethanol The increase in K_{eq} for **PEG-CBCA** compared to **PEG-BCA** indicated that k_1 was accelerated due to the nitrile substituent. We therefore determined the kinetic parameters by monitoring the decrease in conjugate acceptor absorbance upon introduction of β-mercaptoethanol over time and fitting these data to a 2nd order kinetic model that incorporates a 1st order reverse reaction (Equation S2). Similar to the equilibrium experiment discussed above, the formation of the thiol-ene bond breaks the conjugation of the acceptor, shifting the maximum absorbance of the product further away from 300 nm. Indeed, the absorbance of the **PEG-CBCA** decreased faster than that of the **PEG-BCA** upon addition of an equimolar amount of β-mercaptoethanol (Figure 2E). Due to the strong absorption of the reactants, we used low concentrations (20 μM) to stay within the UV/VIS detector range, which in turn yielded low conversions. However, we were still able to quantify the kinetic rate constants by calculating concentration via the Beer-Lambert law and fiting to a two-component addition reaction model (Equation S2) with the forward and reverse reaction rate constants as fitting parameters (Table 1). The addition of an electron withdrawing nitrile group on **PEG-CBCA** led to a 19-fold increase in k_1 as compared to that of **PEG-BCA**: 5.0 x 10^2 ± 50 mol*$L^{-1}s^{-1}$ and 26 ± 1 mol*$L^{-1}s^{-1}$, respectively. In contrast, the reverse reaction rate constant k_{-1} only increased by approximately 6-fold: 0.11 ± 0.007 s^{-1} for **PEG-CBCA** and 0.019 ± 0.0006 s^{-1} for **PEG-BCA**. The equilibrium constants calculated from these data were in excellent agreement with those provided by the equilibrium absorbance measurements. Overall, these results indicated the ability to preferentially tune k_1 with a substituent in the para position of the benzalcyanoacetamide.

Table 1. Rate Constants and Equilibrium Constants of Conjugate Acceptors.

	k_1 ($M^{-1}s^{-1}$)	k_{-1} (s^{-1})	$K_{eq}{}^a$	$K_{eq}{}^b$	G'_∞(Pa)	*Crossover*
PEG-CBCA	$5.0x10^2$±50	0.11±0.007	$4.4x10^3$±400	$4.1x10^3$±600	7500	0.15
PEG-BCA	26±1	0.019±0.0006	$1.3x10^3$±60	$1.2x10^3$±200	2100	0.09
CBCA/BCA	19.2	5.8	3.4	3.4	3.6	1.7

[a] Time resolved absorbance measurement
[b] Equilibrium absorbance measurement
All errors are one standard deviation of experiments ran in triplicate.

Gelation and Mechanical Characterization of Hydrogels We next sought to investigate the impact of tuning the kinetic parameters on the bulk properties of hydrogels crosslinked with this reversible thia-benzalcyanoacetamide conjugate addition. To form hydrogels, 4-arm 20 kDa **PEG-BCA** or **PEG-CBCA** was mixed with a stoichiometric amount of 4-arm 10 kDa PEG-thiol at a functional group concentration of 11.4 mM in water for a 10 wt% gel (Figure 3A). Gelation occurred within seconds, and was too rapid to determine gelation times via shear oscillatory rheometry (Figure 3B). To ensure proper mixing, the hydrogel was prepared by pipetting a solution of PEG-

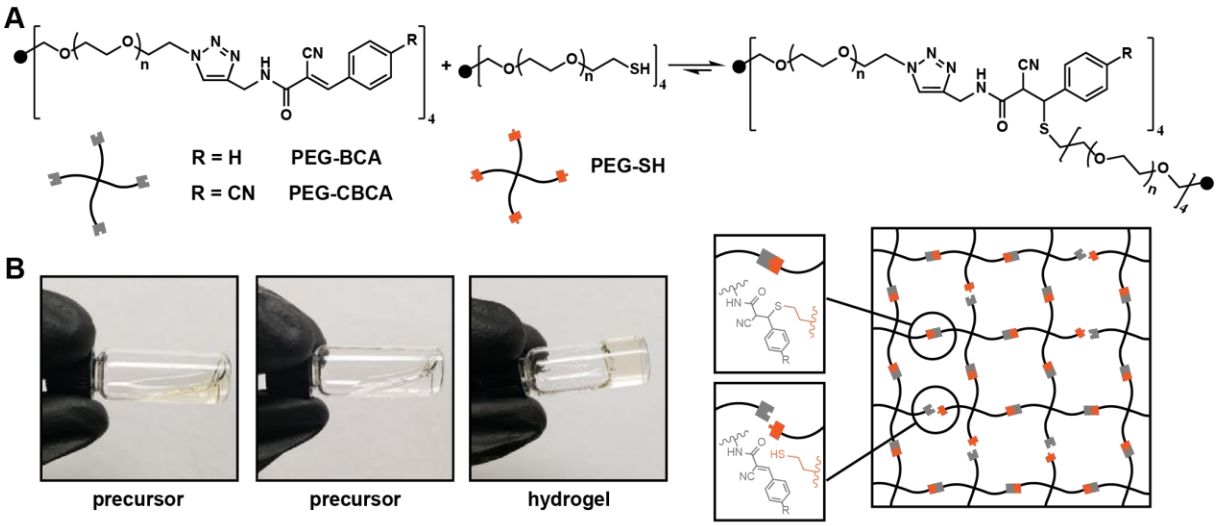

Figure 3. Hydrogel formation using two multi-arm PEG crosslinkers. (A) The reaction between the conjugate acceptor functionalized PEG and a 4-arm PEG-thiol. The substitution of the small molecule thiol for a multi-arm thiol creates a network when reacted. (B) Mixing the two precursor polymer solutions together creates a hydrogel. A cartoon schematic of an idealized network with the bonds in either a crosslinked or a non-crosslinked state demonstrates the dynamic network.

thiol into a solution of the conjugate acceptor functionalized PEG. Due to fast gelation, the hydrogels were mixed post-gelation gently in situ. Because the crosslinks are dynamic, any defects created during this mixing were eliminated as the hydrogel healed.

To characterize the viscoelastic nature of the hydrogels, both a frequency sweep and stress relaxation study were performed on a rheometer. The frequency sweep measures the shear storage (G') and loss (G") moduli of the hydrogels at variable frequencies, ranging from 0.01 to 10 radians per seconds. Due to the dynamic nature of the crosslinks, the network can rearrange and alleviate network stress resulting from the applied shear forces. The frequency of rotation and bond kinetics both influence the measured storage and loss moduli. With a sufficiently low rotational frequency relative to the bond kinetics, the hydrogel can dissipate the majority of any accumulated shear stress, leading to a G" that is higher than G'. In this case, the hydrogel is acting as a viscous liquid rather than an elastic solid. At high rotational frequencies relative to the bond kinetics, the crosslinks do not have sufficient time to rearrange, and the hydrogel accumulates stress along the polymer chains. This leads to a G' that is higher than G", wherein the hydrogel acts as an elastic solid. Both the **PEG-CBCA** and **PEG-BCA** hydrogels exhibit this type of viscoelastic behavior (Figure 4A and B). Additionally, at sufficiently high frequencies (> 1 rad/s), the plateau modulus (G'_∞) is reached, which is the maximum storage modulus achievable for the network based on the crosslinking density (a function of the equilibrium constant of the crosslinking reaction). The **PEG-CBCA** gels reached a higher G'_∞ of 7500 Pa as compared to that of the **PEG-BCA** gels at 2100 Pa (Table 1). As expected, the larger equilibrium constant for the CBCA conjugate acceptor led to a higher G'_∞, as more crosslinks are present at any given time.

The frequency sweep also provides insight to the bulk relaxation behavior of the hydrogel at the crossover point of G' and G". The crossover point can be used as a marker for transition from a viscous liquid to an elastic solid. The faster rate kinetics for the **PEG-CBCA** hydrogels led to a slightly larger crossover point, 0.15 rad/s, compared to 0.09 rad/s for the **PEG-BCA** hydrogels. Compared to the larger difference in plateau modulus, the crossover points for the two hydrogels

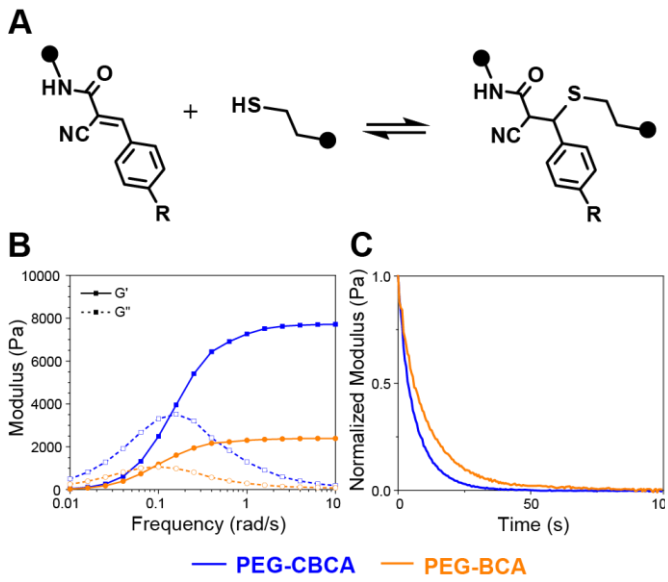

Figure 4. Mechanical testing of both conjugate acceptors. **PEG-BCA** is in orange, and **PEG-CBCA** is in blue. (A) Schematic for the reaction between conjugate acceptor functionalized PEG and thiol functionalized PEG. (B) A frequency sweep of both conjugate acceptors. At sufficiently high frequencies (>1 rad/s), both networks behave as elastic solids, but **PEG-CBCA** shows a higher plateau modulus as a result of its larger equilibrium coefficient. The crossover point between G' and G" for both molecules is around the same mark (~ 0.1 rad/s). (C) This shows the normalized stress relaxation of both molecules through time. When fit to an exponential decay model, the half-life for **PEG-BCA** was 7.5 seconds, and the half-life for **PEG-CBCA** was 4.4 seconds.

were more similar (~1.7 fold difference) (Table 1). This can be attributed to the smaller difference between the reverse rate constants, k_{-1}, of the two molecules. Because stress is only alleviated when a crosslink is broken, and the transition between a viscous liquid and elastic solid depends on this breaking, the crossover point is directly related to the reverse bond kinetics. In summary, the relatively small increase in k_{-1} between **PEG-BCA** and **PEG-CBCA** correlates with the small difference in crossover point.

To further probe the similarity in dissociation kinetics, a stress relaxation test was performed. During this experiment, the instrument rotates to a fixed strain and measures the shear stress over time. Due to the dynamic crosslinking in these hydrogels, the stress will spontaneously dissipate (Figure 4C). By fitting an exponential decay model to the data, a half-life of stress relaxation can be determined. In agreement with the crossover point data from the frequency sweep experiment, the **PEG-CBCA** hydrogels had a slightly faster half-life (4.4 seconds) than the **PEG-BCA** hydrogels (7.5 seconds). Again, the **PEG-CBCA** reaction has a higher k_{-1}, which leads to the modest increase in relaxation for the **PEG-CBCA** hydrogel. Overall, the relaxation time-scales for these two molecules are on the same order of magnitude, which is in contrast to other reversible covalent crosslinks where

changes can lead to a difference of relaxation from seconds to hours.[33] Taken together, these data show the ability to control G'_∞ while maintaining similar stress relaxation, a property that may be useful in applications such as tissue engineering.

Self-Healing Due to the continuous rearrangement of bonds, the synthesized hydrogels demonstrate self-healing behavior, where defects or cuts repair upon contact. Bonds on one side of the defect can separate, and re-form across the defect. Because the exchange kinetics for this thia-conjugate addition reaction are rapid, complete self-healing for this material occurs on the order of minutes. A qualitative example of this healing is shown in Figure 5A. Two hydrogels using the **PEG-CBCA** and PEG-thiol macromers were dyed with red and blue dyes, respectively. They were each cut in half and opposite sides were placed together. After one minute, the hydrogel

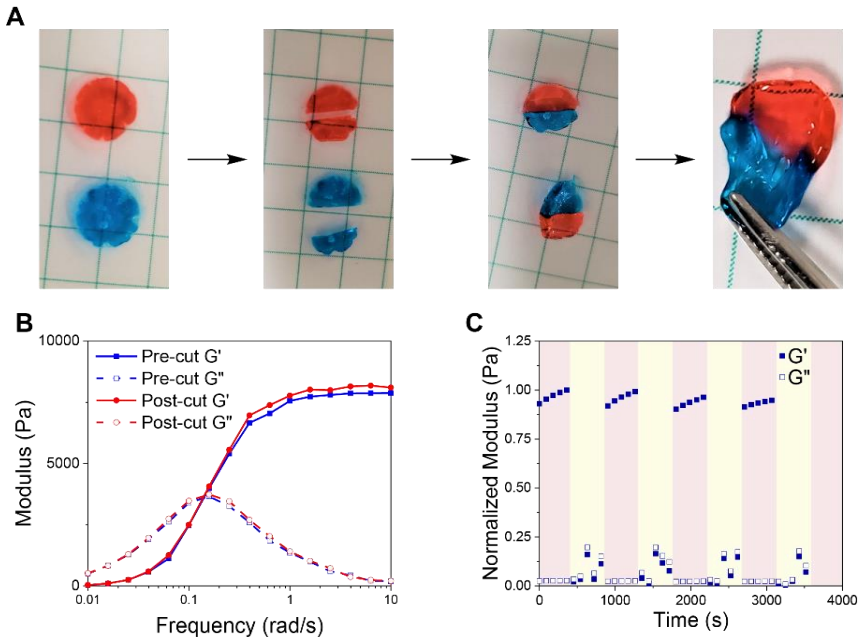

Figure 5. Self-healing behavior of the hydrogels (A) Two hydrogels made with the **PEG-CBCA** molecule were dyed with red and blue food coloring. Each was cut in half and then matched to an opposing colored half. After one minute, the hydrogel healed the cut, and was able to be pulled without tearing. (B) A frequency sweep of the hydrogels before being cut, and after being self-healed, shows that the mechanical properties are fully recovered. (C) The storage modulus is shown as a function of time in multiple strain regimes. Transitions between high strain regimes (yellow, 500%) and low strain regimes (red, 0.5%) while held at a constant frequency of 10 rad/s demonstrate the self-healing nature of the hydrogel. High strain ruptures the hydrogel leading to a sharp decrease in the storage modulus, while the storage modulus is recovered during the low strain regimes.

had reformed across the cut into a continuous material, as demonstrated by the final image that shows the hydrogel stretching when pulled by forceps.

Furthermore, the frequency-dependent shear moduli demonstrated excellent agreement for the pre-cut and post-cut hydrogels (Figure 5B). In addition, exposure to repeated high and low strain (500% and 0.5%, respectively) oscillation tests further demonstrate the self-healing behavior (Figure 5C). Under regions of high strain (yellow highlighted regions), the hydrogel will tear, as demonstrated by the decrease in storage modulus. Subsequent low strain regions (red highlighted regions) allow for the hydrogel to self-heal, as indicated by the recovery of the storage modulus. Multiple trials demonstrate that this self-healing behavior is repeatable, and suggest utility for these materials in applications involving high strain such as 3D printing.

Conclusions

We have demonstrated that reversible thia-conjugate addition offers a highly tunable avenue for hydrogels crosslinked with reversible covalent bonds. The progressive synthesis of the PEG macromer enables easy access to benzalcyanoacetamides with various aromatic substituents, which allows for a modular synthesis that increases accessibility to a tunable range of molecular kinetics. In this work, we focused on a strong electron withdrawing group (nitrile, **PEG-CBCA**) and a neutral directing group (hydrogen, **PEG-BCA**) to probe the effect of bond exchange kinetics on hydrogel properties. As hypothesized, the strongly electron withdrawing group led to faster kinetics in the both the forward and reverse directions. More impactful, however, was that the forward rate constant increased by a factor of nearly twenty, while the reverse rate only increased by a factor of approximately six. When comparing the viscoelasticity of the resulting two hydrogels, those containing **PEG-CBCA** demonstrated a markedly higher plateau modulus, while the stress relaxation characteristics were more similar between the two hydrogels. These results demonstrate that tuning the individual kinetic rate constants for the reversible crosslinks in a polymer network enable decoupling of the resulting material mechanics. The additional kinetic

control outlined in this work will enable the design of hydrogels with highly tailored moduli, stress relaxation, and self-healing behavior for applications in which dynamic properties are important.

Supporting Information

Supporting Information is available free of charge and includes ^{1}H NMR spectra, UV-VIS absorbance data, reactant and product extinction coefficient data, hydrolysis data for the PEG precursors, and kinetic model calculations.

Author Information

Corresponding Author

* E-mail: arosales@che.utexas.edu

ORCID

Eric V. Anslyn 0000-0002-5137-8797

Adrianne M. Rosales 0000-0003-0207-7661

Notes

The authors declare no competing financial interest.

Acknowledgments

This research was supported by the National Science Foundation (NSF MRSEC DMR-1720595, T.M.F., E.V.A., and A.M.R) and by the Burroughs Wellcome Fund (CASI-1015895, A.M.R). The authors acknowledge the use of shared research facilities supported in part by the Texas Materials Institute, the Center for Dynamics and Control of Materials: an NSF MRSEC (DMR-1720595), and the NSF National Nanotechnology Coordinated Infrastructure (ECCS-1542159).

References

(1) Chaudhuri, O.; Gu, L.; Klumpers, D.; Darnell, M.; Bencherif, S. A.; Weaver, J. C.; Huebsch, N.; Lee, H. P.; Lippens, E.; Duda, G. N.; et al. Hydrogels with Tunable Stress Relaxation Regulate Stem Cell Fate and Activity. *Nat. Mater.* **2016**, *15* (3), 326–334. https://doi.org/10.1038/nmat4489.

(2) Purcell, B. P.; Lobb, D.; Charati, M. B.; Dorsey, S. M.; Wade, R. J.; Zellars, K. N.; Doviak, H.; Pettaway, S.; Logdon, C. B.; Shuman, J. A.; et al. Injectable and Bioresponsive Hydrogels for On-Demand Matrix Metalloproteinase Inhibition. *Nat. Mater.* **2014**, *13* (6), 653–661. https://doi.org/10.1038/nmat3922.

(3) Rosales, A. M.; Anseth, K. S. The Design of Reversible Hydrogels to Capture Extracellular Matrix Dynamics. *Nat. Rev. Mater.* **2016**, *1* (2), 1–15. https://doi.org/10.1038/natrevmats.2015.12.

(4) Tang, S.; Ma, H.; Tu, H.; Wang, H.; Lin, P.; Anseth, K. S. Adaptable Fast Relaxing Boronate-Based Hydrogels for Probing Cell – Matrix Interactions. *Adv. Sci.* **2018**, *1800638*, 1–8. https://doi.org/10.1002/advs.201800638.

(5) Wang, H.; Heilshorn, S. C. Adaptable Hydrogel Networks with Reversible Linkages for Tissue Engineering. *Adv. Mater.* **2015**, *27*, 3717–3736. https://doi.org/10.1002/adma.201501558.

(6) Loebel, C.; Rodell, C. B.; Chen, M. H.; Burdick, J. A. Shear-Thinning and Self-Healing Hydrogels as Injectable Therapeutics and for 3D-Printing. *Nat. Protoc.* **2017**, *12* (8), 1521–1541. https://doi.org/10.1038/nprot.2017.053.

(7) Webber, M. J.; Appel, E. A.; Meijer, E. W.; Langer, R. Supramolecular Biomaterials. *Nat. Mater.* **2015**, *15* (1), 13–26. https://doi.org/10.1038/nmat4474.

(8) McKinnon, D. D.; Domaille, D. W.; Brown, T. E.; Kyburz, K. A.; Kiyotake, E.; Cha, J. N.; Anseth, K. S. Measuring Cellular Forces Using Bis-Aliphatic Hydrazone Crosslinked Stress-Relaxing Hydrogels. *Soft Matter* **2014**, *10* (46), 9230–9236.

https://doi.org/10.1039/C4SM01365D.

(9) Kloxin, C. J.; Bowman, C. N. Covalent Adaptable Networks: Smart, Reconfigurable and Responsive Network Systems. *Chem. Soc. Rev.* **2013**, *42*, 7161–7173. https://doi.org/10.1039/c3cs60046g.

(10) Lou, J.; Stowers, R.; Nam, S.; Xia, Y.; Chaudhuri, O. Stress Relaxing Hyaluronic Acid-Collagen Hydrogels Promote Cell Spreading , Fiber Remodeling , and Focal Adhesion Formation in 3D Cell Culture. *Biomaterials* **2018**, *154*, 213–222. https://doi.org/10.1016/j.biomaterials.2017.11.004.

(11) Deng, C. C.; Brooks, W. L. A.; Abboud, K. A.; Sumerlin, B. S. Boronic Acid-Based Hydrogels Undergo Self-Healing at Neutral and Acidic PH. *ACS Macro Lett.* **2015**, *4* (2), 220–224. https://doi.org/10.1021/acsmacrolett.5b00018.

(12) Tseng, T.; Tao, L.; Hsieh, F.; Wei, Y.; Chiu, I.; Hsu, S. An Injectable , Self-Healing Hydrogel to Repair the Central Nervous System. *Adv. Mater.* **2015**, *27*, 3518–3524. https://doi.org/10.1002/adma.201500762.

(13) Zhao, X.; Wu, H.; Guo, B.; Dong, R.; Qiu, Y.; Ma, P. X. Antibacterial Anti-Oxidant Electroactive Injectable Hydrogel as Self- Healing Wound Dressing with Hemostasis and Adhesiveness for Cutaneous Wound Healing. *Biomaterials* **2017**, *122*, 34–47. https://doi.org/10.1016/j.biomaterials.2017.01.011.

(14) Wei, Z.; Yang, J. H.; Du, X. J.; Xu, F.; Zrinyi, M.; Osada, Y.; Li, F.; Chen, Y. M. Dextran-Based Self-Healing Hydrogels Formed by Reversible Diels–Alder Reaction under Physiological Conditions. *Macromolecular Rapid Communications*. 2013, pp 1464–1470. https://doi.org/10.1002/marc.201300494.

(15) Rodell, C. B.; Jr, J. W. M.; Dorsey, S. M.; Wade, R. J.; Wang, L. L.; Woo, Y. J.; Burdick, J. A. Shear-Thinning Supramolecular Hydrogels with Secondary Autonomous Covalent Crosslinking to Modulate Viscoelastic Properties In Vivo. *Adv. Funct. Mater.* **2015**, *25*, 636–644. https://doi.org/10.1002/adfm.201403550.

(16) Yesilyurt, V.; Webber, M. J.; Appel, E. A.; Godwin, C.; Langer, R.; Anderson, D. G. Injectable Self-Healing Glucose-Responsive Hydrogels with PH-Regulated Mechanical Properties. *Adv. Mater.* **2016**, *28* (1), 86–91. https://doi.org/10.1002/adma.201502902.

(17) Wang, H.; Zhu, D.; Paul, A.; Cai, L.; Enejder, A.; Yang, F.; Heilshorn, S. C. Covalently Adaptable Elastin-Like Protein–Hyaluronic Acid (ELP–HA) Hybrid Hydrogels with Secondary Thermoresponsive Crosslinking for Injectable Stem Cell Delivery. *Adv. Funct. Mater.* **2017**, *27* (28), 1–11. https://doi.org/10.1002/adfm.201605609.

(18) Grindy, S. C.; Learsch, R.; Mozhdehi, D.; Cheng, J.; Barrett, D. G.; Guan, Z.; Messersmith, P. B.; Holten-Andersen, N. Control of Hierarchical Polymer Mechanics with Bioinspired Metal-Coordination Dynamics. *Nat. Mater.* **2015**, *14* (12), 1210–1216. https://doi.org/10.1038/nmat4401.

(19) Fadeev, M.; Davidson-rozenfeld, G.; Biniuri, Y.; Yakobi, R.; Cazelles, R.; Aleman-garcia, M. A.; Willner, I. Redox-Triggered Hydrogels Revealing Switchable Stiffness Properties and Shape-Memory Functions. *Polym. Chem.* **2018**. https://doi.org/10.1039/c8py00515j.

(20) Tang, S.; Glassman, M. J.; Li, S.; Socrate, S.; Olsen, B. D. Oxidatively Responsive Chain Extension to Entangle Engineered Protein Hydrogels. *Macromolecules* **2014**, *47* (2), 791–799. https://doi.org/doi:10.1021/ma401684w.

(21) Cui, J.; Campo, A. Del. Multivalent H-Bonds for Self-Healing Hydrogels. *Chem. Commun.* **2012**, *48* (74), 9302–9304. https://doi.org/10.1039/c2cc34701f.

(22) Guo, M.; Pitet, L. M.; Wyss, H. M.; Vos, M.; Dankers, P. Y. W.; Meijer, E. W. Tough Stimuli-Responsive Supramolecular Hydrogels with Hydrogen-Bonding Network Junctions. *J. Am. Chem. Soc.* **2014**, *136* (19), 6969–6977. https://doi.org/10.1021/ja500205v.

(23) Dankers, P. Y. W.; Hermans, T. M.; Baughman, T. W.; Kamikawa, Y.; Kieltyka, R. E.; Bastings, M. M. C.; Janssen, H. M.; Sommerdijk, N. A. J. M.; Larsen, A.; Van Luyn, M. J. A.; et al. Hierarchical Formation of Supramolecular Transient Networks in Water: A

Modular Injectable Delivery System. *Adv. Mater.* **2012**, *24* (20), 2703–2709. https://doi.org/10.1002/adma.201104072.

(24) Zhang, G.; Chen, Y.; Deng, Y.; Ngai, T.; Wang, C. Dynamic Supramolecular Hydrogels: Regulating Hydrogel Properties through Self-Complementary Quadruple Hydrogen Bonds and Thermo-Switch. *ACS Macro Lett.* **2017**, *6* (7), 641–646. https://doi.org/10.1021/acsmacrolett.7b00275.

(25) Rodell, C. B.; Mealy, J. E.; Burdick, J. A. Supramolecular Guest-Host Interactions for the Preparation of Biomedical Materials. *Bioconjug. Chem.* **2015**, *26* (12), 2279–2289. https://doi.org/10.1021/acs.bioconjchem.5b00483.

(26) Appel, E. A.; Biedermann, F.; Hoogland, D.; Del Barrio, J.; Driscoll, M. D.; Hay, S.; Wales, D. J.; Scherman, O. A. Decoupled Associative and Dissociative Processes in Strong yet Highly Dynamic Host-Guest Complexes. *J. Am. Chem. Soc.* **2017**, *139* (37), 12985–12993. https://doi.org/10.1021/jacs.7b04821.

(27) Zou, L.; Braegelman, A. S.; Webber, M. J. Dynamic Supramolecular Hydrogels Spanning an Unprecedented Range of Host-Guest Affinity. *ACS Appl. Mater. Interfaces* **2019**, *11*, 5695–5700. https://doi.org/10.1021/acsami.8b22151.

(28) Jin, Y.; Yu, C.; Denman, R. J.; Zhang, W. Recent Advances in Dynamic Covalent Chemistry. *Chem. Soc. Rev.* **2013**, *42* (16), 6634–6654. https://doi.org/10.1039/c3cs60044k.

(29) Cromwell, O. R.; Chung, J.; Guan, Z. Malleable and Self-Healing Covalent Polymer Networks through Tunable Dynamic Boronic Ester Bonds. *J. Am. Chem. Soc.* **2015**, *137* (20), 6492–6495. https://doi.org/10.1021/jacs.5b03551.

(30) Boehnke, N.; Cam, C.; Bat, E.; Segura, T.; Maynard, H. D. Imine Hydrogels with Tunable Degradability for Tissue Engineering. *Biomacromolecules* **2015**, *16* (7), 2101–2108. https://doi.org/10.1021/acs.biomac.5b00519.

(31) Mckinnon, D. D.; Domaille, D. W.; Cha, J. N.; Anseth, K. S. Bis-Aliphatic Hydrazone-

Linked Hydrogels Form Most Rapidly at Physiological PH: Identifying the Origin of Hydrogel Properties with Small Molecule Kinetic Studies. *Chem. Mater.* **2014**, No. 26, 2382–2387. https://doi.org/10.1021/cm5007789.

(32) Ghobril, C.; Charoen, K.; Rodriguez, E. K.; Nazarian, A.; Grinstaff, M. W. A Dendritic Thioester Hydrogel Based on Thiol – Thioester Exchange as a Dissolvable Sealant System for Wound Closure. *Angew. Chem. Int. Ed.* **2013**, No. 52, 14070–14074. https://doi.org/10.1002/anie.201308007.

(33) McKinnon, D. D.; Domaille, D. W.; Cha, J. N.; Anseth, K. S. Biophysically Defined and Cytocompatible Covalently Adaptable Networks as Viscoelastic 3d Cell Culture Systems. *Adv. Mater.* **2014**, *26* (6), 865–872. https://doi.org/10.1002/adma.201303680.

(34) Koivusalo, L.; Karvinen, J.; Sorsa, E.; Jönkkäri, I.; Väliaho, J.; Kallio, P.; Ilmarinen, T.; Miettinen, S.; Skottman, H.; Kellomäki, M. Hydrazone Crosslinked Hyaluronan-Based Hydrogels for Therapeutic Delivery of Adipose Stem Cells to Treat Corneal Defects. *Mater. Sci. Eng. C* **2018**, *85*, 68–78. https://doi.org/10.1016/j.msec.2017.12.013.

(35) Smithmyer, M. E.; Deng, C. C.; Cassel, S. E.; Levalley, P. J.; Sumerlin, B. S.; Kloxin, A. M. Self-Healing Boronic Acid-Based Hydrogels for 3D Co-Cultures. *ACS Macro Lett.* **2018**, *7* (9), 1105–1110. https://doi.org/10.1021/acsmacrolett.8b00462.

(36) Dufort, B. M.; Tibbitt, M. W. Design of Moldable Hydrogels for Biomedical Applications Using Dynamic Covalent Boronic Esters. *Mater. Today Chem.* **2019**, *12*, 16–33. https://doi.org/10.1016/j.mtchem.2018.12.001.

(37) Jansen, L. E.; Negrón-Piñeiro, L. J.; Galarza, S.; Peyton, S. R. Control of Thiol-Maleimide Reaction Kinetics in PEG Hydrogel Networks. *Acta Biomater.* **2018**, *70*, 120–128. https://doi.org/10.1016/j.actbio.2018.01.043.

(38) Yesilyurt, V.; Ayoob, A. M.; Appel, E. A.; Borenstein, J. T.; Langer, R.; Anderson, D. G. Mixed Reversible Covalent Crosslink Kinetics Enable Precise, Hierarchical Mechanical Tuning of Hydrogel Networks. *Adv. Mater.* **2017**, *29* (19), 1–6.

https://doi.org/10.1002/adma.201605947.

(39) Lou, J.; Liu, F.; Lindsay, C. D.; Chaudhuri, O.; Heilshorn, S. C. Dynamic Hyaluronan Hydrogels with Temporally Modulated High Injectability and Stability Using a Biocompatible Catalyst. *Adv. Mater.* **2018**, *1705215*, 1–6. https://doi.org/10.1002/adma.201705215.

(40) Accardo, J. V.; Kalow, J. A. Reversibly Tuning Hydrogel Stiffness through Photocontrolled Dynamic Covalent Crosslinks. *Chem. Sci.* **2018**, *9* (27), 5987–5993. https://doi.org/10.1039/c8sc02093k.

(41) Fairbanks, B. D.; Schwartz, M. P.; Halevi, A. E.; Nuttelman, C. R.; Bowman, C. N.; Anseth, K. S. A Versatile Synthetic Extracellular Matrix Mimic via Thiol-Norbornene Photopolymerization. *Adv. Mater.* **2009**, *21* (48), 5005–5010. https://doi.org/10.1002/adma.200901808.

(42) Kharkar, P. M.; Kiick, K. L.; Kloxin, A. M. Design of Thiol- and Light-Sensitive Degradable Hydrogels Using Michael-Type Addition Reactions. *Polym. Chem.* **2015**, *6* (31), 5565–5574. https://doi.org/10.1039/c5py00750j.

(43) Hiemstra, C.; van der Aa, L. J.; Zhong, Z.; Dijkstra, P. J.; Feijen, J. Rapidly in Situ-Forming Degradable Hydrogels from Dextram Triols through Michael Addition. *Biomacromolecules* **2007**, *8* (5), 1548–1556. https://doi.org/10.1021/bm061191m.

(44) Hiemstra, C.; Van Der Aa, L. J.; Zhong, Z.; Dijkstra, P. J.; Feijen, J. Novel in Situ Forming, Degradable Dextran Hydrogels by Michael Addition Chemistry: Synthesis, Rheology, and Degradation. *Macromolecules* **2007**, *40* (4), 1165–1173. https://doi.org/10.1021/ma062468d.

(45) Shi, B.; Greaney, M. F. Reversible Michael Addition of Thiols as a New Tool for Dynamic Combinatorial Chemistry. *Chem. Commun.* **2005**, No. 7, 886–888. https://doi.org/10.1039/b414300k.

(46) Krenske, E. H.; Petter, R. C.; Houk, K. N. Kinetics and Thermodynamics of Reversible

Thiol Additions to Mono- and Diactivated Michael Acceptors: Implications for the Design of Drugs That Bind Covalently to Cysteines. *J. Org. Chem.* **2016**, No. 81, 11726–11733. https://doi.org/10.1021/acs.joc.6b02188.

(47) Zhong, Y.; Xu, Y.; Anslyn, E. V. Studies of Reversible Conjugate Additions. *European J. Org. Chem.* **2013**, No. 23, 5017–5021. https://doi.org/10.1002/ejoc.201300358.

(48) Kuhl, N.; Geitner, R.; Bose, R. K.; Bode, S.; Dietzek, B.; Schmitt, M.; Popp, J.; Garcia, S. J.; Zwaag, S. Van Der; Schubert, U. S.; et al. Self-Healing Polymer Networks Based on Reversible Michael Addition Reactions. *Macromol. Chem. Phys.* **2016**, *217*, 2541–2550.

(49) Bode, S.; Schmitt, M.; Kuhl, N.; Geitner, R.; Schubert, U. S.; Hager, M. D. Increased Stability in Self-Healing Polymer Networks Based on Reversible Michael Addition Reactions. *J. Appl. Polym. Sci.* **2017**, *44805*, 1–8. https://doi.org/10.1002/app.44805.